Memory effects in spiral diffusion of rotary self-propellers

Parvin Bayati [1,2] and Amir Nourhani [1,3,4,*]

[1]*Department of Mechanical Engineering, University of Akron, Akron, Ohio 44325, USA*
[2]*Université Paris-Saclay, CNRS, Le Laboratoire de Physique Théorique et Modèles Statistiques, 91405 Orsay, France*
[3]*Biomimicry Research and Innovation Center, University of Akron, Akron, Ohio 44325, USA*
[4]*Departments of Biology, Mathematics, and Chemical, Biomolecular, and Corrosion Engineering, University of Akron, Akron, Ohio 44325, USA*

(Received 10 November 2021; accepted 2 February 2022; published 18 February 2022)

The coupling of deterministic rotary motion and stochastic orientational diffusion of a self-propeller leads to a spiral trajectory of the expected displacement. We extend our former analysis of spiral diffusion [Phys. Rev. E **94**, 030601(R) (2016)] in the white-noise limit to a more realistic scenario of stochastic noise with Gaussian memory and orientational fluctuations driven by an Ornstein-Uhlenbeck process. A variety of dynamical regimes including crossovers from ballistic to diffusive to ballistic in the angular dynamics are determined by the inertial timescale, orientational diffusivity, and angular speed.

DOI: 10.1103/PhysRevE.105.024606

I. INTRODUCTION

Self-propellers range from microorganisms [1–7] and artificial microswimmers [8–12] at the microscale to animals [13–17], insects [18,19], and humans [20,21] at the macroscale. From a statistical perspective, trajectories of self-propellers result from coupling deterministic motion and stochastic dynamics. The former is usually a powered motion in a rectilinear or rotary motion, while the latter originates from thermal noise at microscale and decision-making by the self-propeller to change direction of motion or speed. The resulting trajectories are diverse and can be used to distinguish and classify self-propellers. For example, the expected displacement of a rotary microswimmer follows a spiral path [22–24], whereas run-and-tumble microorganisms like *Escherichia coli* [25,26] perform random walks.

Stochastic forces usually are the main factor in modifying the orientation of self-propellers. Such orientational changes are unavoidable in small scales and may originate from thermal fluctuations, motility mechanism, and food supplies or other complexities in the surroundings [3,4,27–29]. While thermal noises at microscale are usually approximated to be memoryless in Newtonian fluids [1,2,30–32], the memory effects emerge in polymeric and more complex fluids, partly due to the elastic component of dynamics. A self-propeller exhibits ballistic motion at short timescales, whereas its persistent motion is strongly affected by the random changes in its orientation at long times. Consequently, for a microscale self-propeller, coupling of deterministic and stochastic motions results in an enhanced translational diffusion, in addition to passive thermal diffusion [12,33–36].

Recent experiments [17,37,38] show that some microswimmers can resist orientation fluctuations through some internal dynamics. This provides an effective inertia so that their orientation may persist with time, and the stochastic dynamics is better described as driven by correlated (colored) noise rather than memoryless white noise. In other words, the internal dynamics induce memory effects on the orientational motion of active particles [36,39–41]. Moreover, in complex environments memory effects are common features of the interactions of small-scale self-propellers with their surroundings, leading to unexpected phenomena including spontaneous rotational motion of rectilinear symmetric particles in non-Newtonian fluids [42], uniform spreading of active particles instead of condensation at the borders of harmonic confinements [43], and inertia-induced phase separations in motile particles [44].

In addition to rectilinear self-propellers whose powered motion is along a straight trajectory [45–53], microscopic rotary self-propellers [3,4,22,25,27–29,54] moving through curved paths are of particular importance [11,54–57]. This type of micromotor is found among both biological and artificial examples [58–63]. In addition, it has been shown that some linear micromotors swim in curved trajectories in complex environments or when they are confined [17,64–69]. Asymmetric geometry of active particles leads to a driving force misaligned with the drag force, leading to change in particle orientation over time. Typical examples in artificial microswimmers are nominally geometries with a fabrication-induced asymmetry, such as a tilted sphere [10,30], Janus tadpoles [70], and dimers [71]. Such particles travel in a circular trajectories intrinsically. Combining orientational white noise and the deterministic rotation leads to an effective chiral translational diffusion such that the self-propeller tends, on average, to move toward its right or left depending on the chirality of the deterministic rotation [23,41,55,56,72].

The noise effects on chiral swimmers have been studied for white Gaussian noise [23], telegraph process [62], Ornstein-Uhlenbeck (OU) process [73], and time-dependent inertia [63]. Usually, a modeling approach using Fokker-Planck formalism [61,73] or Langevin dynamics

*nourhani@uakron.edu

simulations [59,62,63] has been applied. However, these differential-equation-based approaches require complicated calculations or obtain probability distribution functions. The complexity of Fokker-Planck formalism requires cumbersome mathematical calculations to investigate effective diffusion of a chiral swimmer [61]. Moreover, with increase in the number of degrees of freedom in a system, such analysis gets more complicated. Here we take advantage of kinematic matrix (kinematrix) theory which circumvent the need for calculation of probability distribution functions and facilitates studying dynamics of self-propellers.

We have previously studied orientational OU memory effects on the dynamics of a rectilinear self-propellers [74], and spiral diffusion of rotary self-propellers in the white-noise limit [23], using kinematrix theory. In this paper, we study the effect of OU Gaussian memory and orientational inertia on spiral diffusion of rotary self-propellers. Comparing with the white-noise limit, we investigate how an orientational inertia, modeled by correlated OU process, modifies the dynamics of the self-propeller. While our discussion of effective diffusion may overlap with an earlier study [73], our analysis of spiral dynamics and mean-squared displacement complements that study. Moreover, that study required full knowledge of probability distribution functions while our work circumvents this need and within a simpler framework using a kinematrix formalism directly obtains the quantities of interest. In doing so, we provide a reformulation of kinematrix theory in which we translate the matrix manipulations into the machinery of complex numbers. Our results provides a ground for further analysis of the interplay between different timescales and further analysis of experimental observations.

In our analysis we need the autocorrelations embedded in a time-evolution multiplier to obtain the necessary information, including ensemble average trajectories, effective diffusivity, and mean-squared displacement. We discuss in detail the effects of all relevant timescales on spiral diffusion of the self-propellers and how the inertial timescale modifies the effect of other timescales. The structure of the paper is as follows: First, in Sec. II, we describe the model of circle swimmers subjected to an OU process which implies a memory in particle orientation. We discuss the effect of memory on angular dynamics (Sec. III) and build a time-evolution multiplier (Sec. IV) which is central to the kinematic matrix formalism. Then we study spiral diffusion (Sec. V) by analyzing the expected displacement of the rotary self-propeller. Finally, we discuss how the self-propellers spread by investigating their effective translational diffusivity and, more generally, time-dependent mean-squared displacement (Sec. VI). This analysis gives us information about expected behavior in the presence of the orientational memory in the system, which is summarized in Sec. VII.

II. PROBLEM FORMULATION

The self-propeller moves with time-dependent velocity $\boldsymbol{v}_t \equiv \boldsymbol{v}(t)$ of constant magnitude $v_0 = |\boldsymbol{v}_t|$ in the xy plane while rotating with angular velocity ω. We define chirality $\mathcal{S} = \omega/|\omega|$ which is $+1$ for counterclockwise (CCW) rotation and -1 for clockwise (CW). In the absence of noise the self-propeller follows a circular trajectory of radius $R = v_0/|\omega|$. In the presence of noise the self-propeller's orientation changes according to

$$\frac{d\theta}{dt} = \omega + \lambda, \tag{1}$$

in which λ is a zero-mean stationary Ornstein-Uhlenbeck process (OUP) and η is Gaussian white noise of intensity $\tau_\lambda^{-2} D_o$:

$$d\lambda/dt = -\tau_\lambda^{-1}\lambda(t) + \eta(t), \tag{2a}$$

$$\langle \eta(t)\eta(t')\rangle = 2\tau_\lambda^{-2} D_o \delta(t-t'), \tag{2b}$$

$$\langle \lambda(t)\lambda(0)\rangle = \tau_\lambda^{-1} D_o e^{-|t|/\tau_\lambda}, \tag{2c}$$

where τ_λ is the correlation that quantifies the inertia or memory of the stochastic orientation change and D_o is the orientational diffusivity such that D_o^{-1} describes the timescale that the rotor changes its orientation due to pure Brownian rotation. This model takes into account rotational inertia of the self-propeller which may be caused by internal or external stochastic processes. The coupling of the orientational stochastic dynamics and active translation leads to an effective translational diffusion superposed to the passive translational diffusion in an additive manner. However, while in viscoelastic fluid the strength of the stochastic processes may be influenced by the active motion [42], within our model in a Newtonian fluid passive translational diffusion is not coupled to the rotational and active translational dynamics, and it does not enter the discussion about the interplay between deterministic and stochastic dynamics.

In two dimensions, we represent the position $\boldsymbol{x}$ and velocity $\boldsymbol{v}$ as complex numbers. For example:

$$\boldsymbol{v} = v_x\hat{\boldsymbol{x}} + v_y\hat{\boldsymbol{y}} \;:\to\; v_x + iv_y, \tag{3}$$

where $i = \sqrt{-1}$, and thus we define the dot product between the vectors in the complex plan as

$$\boldsymbol{x}\cdot\boldsymbol{v} := \mathrm{Re}\{\bar{\boldsymbol{x}}\boldsymbol{v}\} \equiv \mathrm{Re}\{\boldsymbol{x}\bar{\boldsymbol{v}}\}, \tag{4}$$

where $\bar{\boldsymbol{x}}$ is the complex conjugate of $\boldsymbol{x}$. The velocity is then identified by constant magnitude v_0 and a time-dependent phases $\theta_v(t)$ in the complex plane, that is,

$$\boldsymbol{v}_t = v_0 \exp[i\,\theta_v(t)]. \tag{5}$$

We are interested in the conditional expectation of $\boldsymbol{v}_{t+\Delta t}$ given $\boldsymbol{v}_t$, that is, what is the expected value of velocity at time $t+\Delta t$ if know the velocity at time t,

$$\mathsf{E}(\boldsymbol{v}_{t+\Delta t}|\boldsymbol{v}_t) = \mathcal{U}(\Delta t)\boldsymbol{v}_t. \tag{6}$$

where $\mathcal{U} = e^{if(t)}$ is a time-evolution multiplier. Since v_0 is constant, rotational invariance and stationarity (time-shift invariance) alone states that $\mathcal{U}$ is well defined by Eq. (6) and nonrandom. Therefore, for the velocity autocorrelation function we have

$$\begin{aligned}\mathsf{E}(\boldsymbol{v}_{t'+t}\cdot\boldsymbol{v}_t|\boldsymbol{v}_t) &= \mathsf{E}(\mathrm{Re}\{\boldsymbol{v}_{t'+t}\bar{\boldsymbol{v}}_t\}|\boldsymbol{v}_t)\\ &= \mathrm{Re}\{\mathsf{E}(\boldsymbol{v}_{t'+t}|\boldsymbol{v}_t)\bar{\boldsymbol{v}}_t\} = v_0^2\mathrm{Re}\{\mathcal{U}(t'-t)\},\end{aligned} \tag{7}$$

which is proportional to the real part of the time-evolution multiplier.

By setting the reference point as the initial position of the self-propeller, that is, $\boldsymbol{x}_0 = 0$, the conditional expectation of

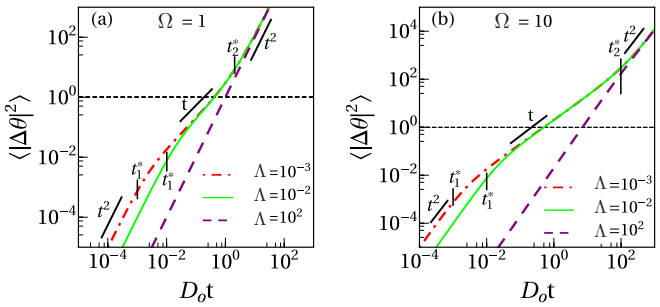

FIG. 1. Angular dynamics of rotating self-propeller with Ornstein-Uhlenbeck orientational dynamics. In the regime $\Lambda < \Omega^2$ we have two crossovers from ballistic to diffusive to ballistic while in the regime $\Lambda > \Omega^2$ we only have ballistic dynamics.

displacement given initial velocity $\boldsymbol{v}_0$ is

$$\mathsf{E}(\boldsymbol{x}_t|\boldsymbol{v}_0) = \int_0^t \mathsf{E}(\boldsymbol{v}_{t'}|\boldsymbol{v}_0)\,dt' = \boldsymbol{v}_0 \int_0^t \mathcal{U}(t')\,dt' \tag{8}$$

and using (7) the conditional expectation of the mean-squared displacement (MSD) is expressed as

$$\begin{aligned}\mathsf{E}(|\boldsymbol{x}_t|^2|\boldsymbol{v}_0) &= 2\int_0^t dt' \int_0^{t'} dt''\, \mathsf{E}(\boldsymbol{v}_{t''}\cdot\boldsymbol{v}_{t'}|\boldsymbol{v}_0) \\ &= 2\mathrm{Re}\left\{\int_0^t dt' \int_0^{t'} dt''\,\mathcal{U}(t'')\right\}. \end{aligned}\tag{9}$$

Therefore, all we are interested in calculating in this paper are obtained by simple operations from $\mathcal{U}(t)$, $\int_0^t dt'\,\mathcal{U}(t')$, and $\int_0^t dt' \int_0^{t'} dt''\,\mathcal{U}(t'')$. In the next section we will discuss how to evaluate these terms for a Gaussian memory.

III. ANGULAR DYNAMICS

The autocorrelation integral for the OUP angular velocity $\mathcal{C}_\lambda^{\mathrm{OUP}}(t) = \int_0^t \int_0^t \langle\lambda(0)\lambda(t'')\rangle dt''dt'$ is monotonically increasing:

$$\mathcal{C}_\lambda^{\mathrm{OUP}}(t) = 2D_o t + 2D_o\tau_\lambda(e^{-t/\tau_\lambda} - 1). \tag{10}$$

The first term is the white-noise contribution and the second term is the modification due to inertia.

The mean-squared angular displacement is

$$\begin{aligned}\langle|\Delta\theta(t)|^2\rangle &= \mathcal{C}_\lambda^{\mathrm{OUP}}(t) + \omega^2 t^2 \\ &\approx \begin{cases}(t/\tau_\lambda)D_o t + \omega^2 t^2 & t \ll \tau_\lambda \\ 2D_o t + \omega^2 t^2 & t \gg \tau_\lambda\end{cases}. \end{aligned}\tag{11}$$

The indicated regimes of rotor orientation dynamics can be seen clearly in the plots of Fig. 1. Since $\Delta\theta(t)$ is the sum of a deterministic part and a zero-mean stochastic part, $\langle|\Delta\theta(t)|^2\rangle$ is also simply the sum of a deterministic and a stochastic contribution. The instantaneous angular velocity $\dot\theta(t)$ is the sum of ω and a normally distributed component of variance D_o/τ_λ. Furthermore, τ_λ is the correlation time of the stochastic component.

We define two dimensionless parameters,

$$\Lambda := D_o\tau_\lambda, \quad \Omega := D_o|\omega|^{-1} := D_o\tau_\omega, \tag{12}$$

that help with analysis of the dynamical regimes. A discretized version which favors qualitative insight by removing analytical complication is this: A random angular velocity is chosen from the distribution indicated above, and it persists for time τ_λ, after which a new, independent, value is chosen. In this version, θ undergoes a biased random walk, with each step a constant-velocity motion. The mean-squared size of the random part of the steps is Λ, and the random part of the motion crosses over from ballistic to diffusive character on the timescale τ_λ. Thus, the motion is ballistic over short timescales $\ll \tau_\lambda$, as it is over very long timescales since the constant ω always wins out over diffusion in the long run, as the second limit in (11) shows.

At this crude level of analysis, the only question is whether the deterministic motion dominates already at τ_λ, in which case the net motion is always ballistic, or whether there is an intermediate diffusive regime. However, for a purely diffusive motion, the crossover time t^* is determined by $D_o t^* = (\omega t^*)^2$, or $D_o t^* = \Omega^2$. So the diffusive regime is $\Lambda < D_o t < \Omega^2$ if this interval is nonempty. Note that since the random component of the instantaneous angular velocity has standard deviation $\sqrt{D_o/\tau_\lambda}$, the diffusive regime exists if the width of the instantaneous angular velocity distribution is large compared to its center $|\omega|$.

Consideration of the disorientation time τ_θ gives a better understanding of the angular dynamics. τ_θ is the time that orientation changes significantly, i.e., $\langle|\Delta\theta(\tau_\theta)|^2\rangle = 1$. The deterministic motion covers an angle 1 in time $D_o\tau_\omega$. For the random component, recall that it is roughly composed of steps of angle $\sqrt{D_o\tau_\lambda}$ at speed $\sqrt{D_o/\tau_\lambda}$. Hence, *if* $D_o\tau_\lambda > 1$, then it covers angle 1 while still in the ballistic regime in a time $\sqrt{\tau_\lambda/D_o}$. Otherwise, it takes longer than τ_λ and we calculate the time as if it were simple diffusion: $D_o t = 1$. Summarizing, $D_o\tau_\theta \sim \min(D_o\tau_\omega, D_o\tau')$, where $D_o\tau'$ is 1 if $D_o\tau_\lambda < 1$; otherwise, $\sqrt{\tau_\lambda/D_o}$.

IV. TIME-EVOLUTION MULTIPLIER

Within the kinematic matrix formalism [74,75] the time-evolution operator takes the form of a multiplier in the complex plane,

$$\begin{aligned}\mathcal{U}(t) = \mathcal{U}(t;\Lambda,D_o,\omega) &= \exp\left[\omega\mathcal{J}_z t - \tfrac{1}{2}\mathcal{C}_\lambda^{\mathrm{OUP}}(t)\mathcal{P}_z^\perp\right] \\ &:\to \exp[-(D_o - i\omega)t - \Lambda(e^{-D_o t/\Lambda} - 1)], \end{aligned}\tag{13}$$

where $\mathcal{J}_z$ is the generator of rotation about $\hat{\boldsymbol{z}}$, $\mathcal{P}_z^\perp$ is projection on the xy plane. In the second line we have converted the matrix formalism to a phase in the complex plane. Note that in the limit $\Lambda \to 0$ we obtain the white-noise limit of the time-evolution multiplier (denoted by "wn"),

$$\mathcal{U}^{\mathrm{wn}}(t) = \mathcal{U}(t;0,D_o,\omega) = \exp[-(D_o - i\omega)t], \tag{14}$$

and in the limit $\tau_\lambda \to \infty$ we have pure rotation $\mathcal{U}(t;\infty,D_o,\omega) = \exp(i\omega t)$ and the self-propeller returns to its initial position after each period of rotation.

Here we show that the evolution multiplier of a self-propeller with Gaussian memory (13) can be written as a linear combination of evolution multipliers in the white-noise

limit (14) by the Taylor expansion of the outer exponential of $\exp[-\Lambda e^{-D_o t/\Lambda}]$:

$$\mathcal{U}(t;\Lambda,D_o,\omega) = e^{\Lambda}\sum_{n=0}^{\infty}\frac{(-\Lambda)^n}{n!}e^{-(D_n-i\omega)t}, \tag{15a}$$

$$= e^{\Lambda}\sum_{n=0}^{\infty}\frac{(-\Lambda)^n}{n!}\mathcal{U}(t;0,D_n,\omega), \tag{15b}$$

where

$$D_n := \alpha_n D_o \quad \text{with} \quad \alpha_n := 1+\tfrac{n}{\Lambda} \tag{16}$$

is a sequence of ever-increasing "effective" diffusion coefficients. From Eqs. (8) and (9) we learn that $\mathsf{E}(\boldsymbol{x}_t|\boldsymbol{v}_0)$ and $\mathsf{E}(|\boldsymbol{x}_t|^2|\boldsymbol{v}_0)$ are linear in $\mathcal{U}$, and to calculate them we can take the integration into the summation when using Eq. (15). Therefore, the expected displacement and MSD for a rotary self-propeller undergoing OU process is also a linear combination of these quantities for white-noise limits with effective orientational diffusivities D_n.

V. SPIRAL DIFFUSION

We start with finding the expected displacement for the white-noise limit using Eq. (14),

$$\mathsf{E}\big(\boldsymbol{x}_t^{\rm wn}|\boldsymbol{v}_0\big) = \boldsymbol{v}_0\int_0^t \mathcal{U}^{\rm wn}(t')dt' = \boldsymbol{v}_0\Psi(t;D_o,\omega), \tag{17}$$

where we have defined the function

$$\Psi(t;D_o,\omega) = \frac{1}{D_o-i\omega}[1-e^{-(D_o-i\omega)t}]. \tag{18}$$

We discuss chiral diffusion by studying the limit $t\to\infty$ and then the spiral diffusion in the next section by analyzing the intermediate regime. The asymptotic long-time behavior for the expected displacement of the self-propeller for the white-noise limit is

$$\mathsf{E}(\boldsymbol{x}_\infty^{\rm wn}|\boldsymbol{v}_0) = \boldsymbol{v}_0\Psi(\infty;D_o,\omega) \equiv \boldsymbol{v}_0\frac{D_o+i\omega}{D_o^2+\omega^2}$$

$$= Re^{i\theta_v(0)}\frac{\Omega+i\mathcal{S}}{\Omega^2+1}. \tag{19}$$

Similarly, the asymptotic value of the expected displacement for self-propeller with OU process is the linear combination [see (16) for D_n and α_n]

$$\mathsf{E}(\boldsymbol{x}_\infty|\boldsymbol{v}_0) = \boldsymbol{v}_0 e^{\Lambda}\sum_{n=0}^{\infty}\frac{(-\Lambda)^n}{n!}\frac{D_n+i\omega}{D_n^2+\omega^2}$$

$$= Re^{i\theta_v(0)}\,e^{\Lambda}\sum_{n=0}^{\infty}\frac{(-\Lambda)^n}{n!}\left(\frac{\alpha_n\Omega+i\mathcal{S}}{\alpha_n^2\Omega^2+1}\right). \tag{20}$$

We define the chiral angle ϕ_∞ as the angle between $\boldsymbol{v}_0$ and $\mathsf{E}(\boldsymbol{x}_\infty|\boldsymbol{v}_0)$. In the white-noise limit, from Eq. (19) we have

$$\phi_\infty^{\rm wn} = \tan^{-1}(\omega/D_o) = \mathcal{S}\cot^{-1}(\Omega). \tag{21}$$

Depending on the sign of ω, and thus the self-propeller's chirality $\mathcal{S}$, the chiral angle is added to or subtracted from the phase $\theta_{v,0}$ of the initial velocity. As shown in Fig. 2(a) for CW rotation the expected displacement is toward the right

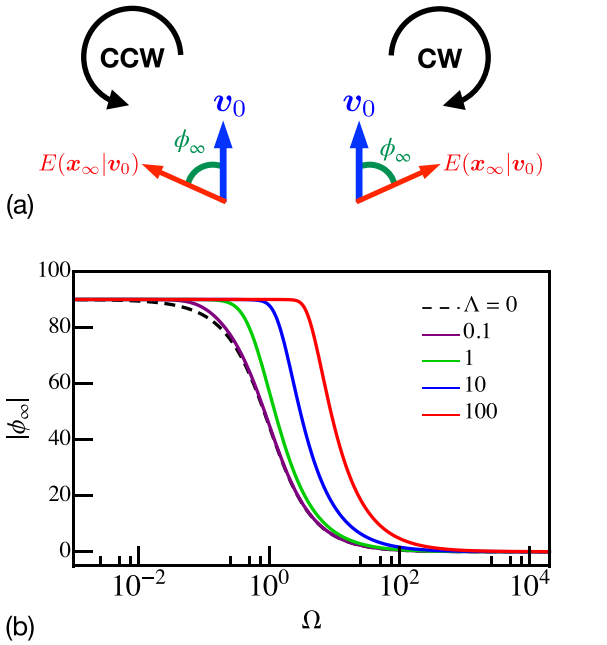

FIG. 2. (a) Dependence of expected displacement on chiral angle. (b) Absolute value of the chiral angle $|\phi_\infty|$ as a function of $D_o\tau_\omega$ for different values of correlation time.

of $\boldsymbol{v}_0$ while for CCW it is toward the left [55,56]. Comparing Eqs. (19) and (20) reveals that a self-propeller with OU process behaves qualitatively similarly to the white-noise limit.

Figure 2(b) shows the absolute value of chiral angle $|\phi_\infty|$ as a function of dimensionless rotational timescale Ω for different values of dimensionless correlation time Λ. The white-noise limit, Eq. (21), holds, and in the limit $|\omega|\gg D_o$ ($\Omega\ll 1$) the deterministic rotation dominates the orientational diffusion, the trajectories are nearly circular and $|\phi_\infty|\approx\pi/2$. In the other extreme, $|\omega|\ll D_o$ ($\Omega\gg 1$), the orientation is changed stochastically much faster than deterministic rotation, the chiral diffusion effects are washed out, and the rotors no longer distinguish right and left. Thus, the chiral angle is nearly zero. On increasing the correlation time, the asymptotic value of chiral angel ϕ_∞ increases for a given Ω.

Next, we discuss the temporal behavior of the expected displacement before reaching its asymptotic values. The expected displacement of the self-propeller with inertia is given by

$$\mathsf{E}(\boldsymbol{x}_t|\boldsymbol{v}_0) = \boldsymbol{v}_0 e^{\Lambda}\sum_{n=0}^{\infty}\frac{(-\Lambda)^n}{n!}\Psi(t;D_n,\omega). \tag{22}$$

In the absence of any noise, i.e., $D_o=0$, we recover the circular deterministic trajectory centered at $i\mathcal{S}Re^{i\theta_{v,0}}$:

$$\mathsf{E}\big(\boldsymbol{x}_t^{\rm det}|\boldsymbol{v}_0\big) = i\mathcal{S}Re^{i\theta_{v,0}}[1-e^{i\omega t}]. \tag{23}$$

By addition of noise ($D_o\neq 0$) the trajectory deviates from circularity. Again, a discrete model helps to portray the physical pictures: In timescales less than D_o^{-1} the rotor rotates on a circular trajectory. At D_o^{-1} it changes its orientation and rotates on the circular trajectory with the new center until

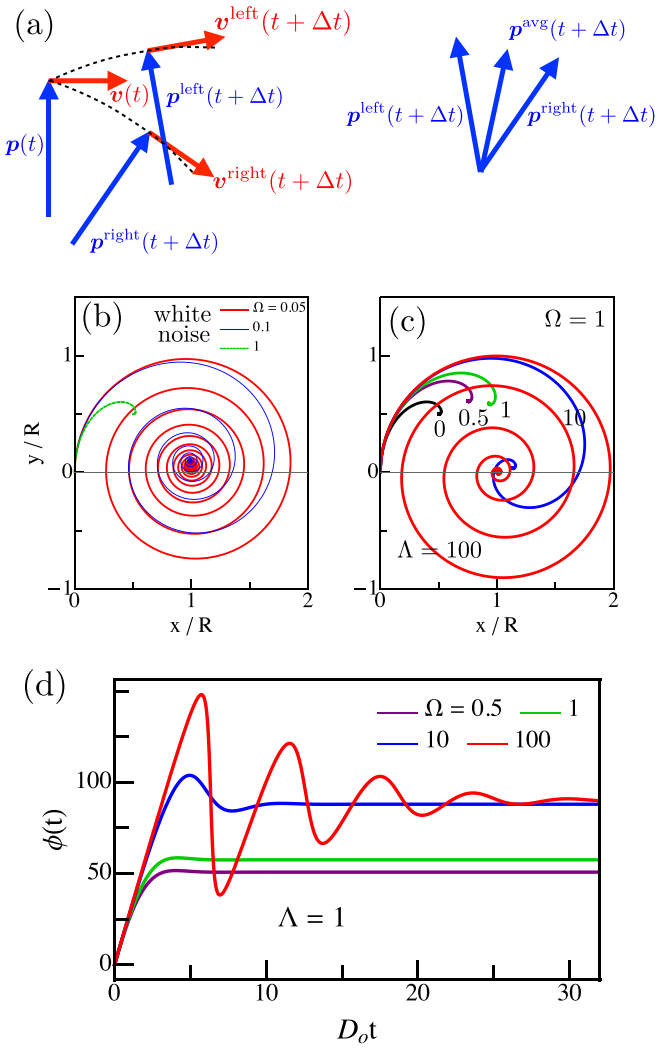

FIG. 3. (a) Average radius of rotation decrease with time leading to (b) spiral pattern in the expected displacement and (c) damped oscillatory behavior for the spiral angle $\phi(t)$.

again it changes its center of rotation. The vector connecting the instantaneous center of rotation to the location of particle at time t is $\boldsymbol{p}(t)$. As shown in Fig. 3(a) the particle may stochastically reorient to its left or right and move ballistically for a time Δt. Then the two vectors $\boldsymbol{p}^{\rm right}(t+\Delta t)$ and $\boldsymbol{p}^{\rm left}(t+\Delta t)$ connecting the centers of rotation to the position of the self-propeller will have an average $\boldsymbol{p}^{\rm avg}(t+\Delta t)$ shorter than either of them. Therefore, on average, the radius of rotation decreases with time and the self-propeller's expected displacement follows a spiral.

Figure 3(b) shows the spiral trajectories in the white-noise limit. At short values of Ω the deterministic motion dominates the stochastic noise and the expected displacement follows a long spiral. With increase of Ω, the stochastic component gets stronger, the average orbital radius decrease faster, and the spiral converges on shorter timescales. On the other hand, in the presence of orientational memory, shown in Fig. 3(c), with an increase in Λ the self-propeller tends to keep its orientation for longer times, the radius of spiral remains larger, and the spiral converges slower. As shown in Fig. 3(d) the angle $\phi(t)$ between the initial velocity $\boldsymbol{v}_0$ and the expected displacement at time t oscillates for high values of Ω enveloped by a decaying behavior while $\phi(t)$ reaches its asymptotic values on short timescales for small inertial correlation time.

VI. MEAN-SQUARED DISPLACEMENT AND EFFECTIVE DIFFUSION

Using Eqs. (9), (14), and (15) we obtain the expression for the mean-squared displacement of the self-propeller,

$$\mathsf{E}(|x_t|^2|\boldsymbol{v}_0) = 2v_0^2 e^{\Lambda}\sum_{n=0}^{\infty}\frac{(-\Lambda)^n}{n!}\mathrm{Re}\{\Phi(t;D_n,\omega)\}, \tag{24}$$

where we have defined the function

$$\Phi(t;D_n,\omega) := \frac{1}{D_n - i\omega}t + \frac{e^{-(D_n-i\omega)t}-1}{(D_n-i\omega)^2}, \tag{25}$$

whose real part is related to the effective diffusion of the self-propeller in the white-noise limit,

$$\lim_{t\to\infty}\mathrm{Re}\left\{\frac{1}{t}\Phi(t;D_o,\omega)\right\} = \mathrm{Re}\left\{\frac{1}{D_o - i\omega}\right\} = \frac{D_o}{D_o^2+\omega^2}. \tag{26}$$

The coupling of the orientational diffusion with deterministic rotation leads to a translational diffusion with an effective diffusivity,

$$D_{\rm eff} = \lim_{t\to\infty} t^{-1}\mathsf{E}(|\boldsymbol{x}_t|^2|\boldsymbol{v}_0) = \frac{v_0^2}{2}e^{\Lambda}\sum_{n=0}^{\infty}\frac{(-\Lambda)^n}{n!}\frac{D_n}{D_n^2+\omega^2}$$

$$= \frac{v_0^2}{2D_o}e^{\Lambda}\sum_{n=0}^{\infty}\frac{(-\Lambda)^n}{n!}\frac{\Omega^2\alpha_n}{\Omega^2\alpha_n^2+1} \tag{27a}$$

$$\approx \begin{cases} \frac{v_0^2}{2D_o}\frac{\Omega^2}{1+\Omega^2}\,e^{\Lambda}, & \Lambda \ll 1 \\ \frac{v_0^2}{2D_o}e^{-\Lambda/2\Omega^2}\sqrt{\frac{\pi\Lambda}{2}}, & \Lambda \gg 1 \end{cases}, \tag{27b}$$

whose behavior is depicted in Fig. 4 for various values of Ω and Λ.

To explain the observed behavior, we start with the simple case of a rectilinear self-propeller moving with constant speed v_0 while suffering a white noise of intensity D_o. The self-propeller experiences an effective diffusion of $D_{\rm eff} = v_0^2/2D_o$. If we add a rotation with angular speed $|\omega| = \tau_\omega^{-1}$, then, using Eq. (26), the resulting effective diffusivity is

$$D_{\rm eff}^{\rm wn} = \frac{v_0^2}{2D_o}\frac{\Omega^2}{1+\Omega^2}, \tag{28}$$

which immediately implies that a finite angular speed always decreases the effective diffusivity compared to the rectilinear scenario.

We understand from Eq. (27) that in the limit $\Omega \ll 1$, the effective diffusivity $D_{\rm eff} \propto \Omega^2 \ll 1$ can be negligible for different values of Λ, as shown in Fig. 4(a). On the other hand, in the limit $\Omega \gg 1 (D_o \gg |\omega|)$ the self-propeller's trajectory deviates significantly from circularity, and thus with increase in the persistent time τ_λ (and thus Λ) the length of steps increases, leading to the increase in the effective diffusivity [see Fig. 4(a)]. We can also investigate the effective diffusivity from the perspective of variation in correlation time, as depicted in Fig. 4(b). In the limit $\Lambda \ll 1$ in the case of

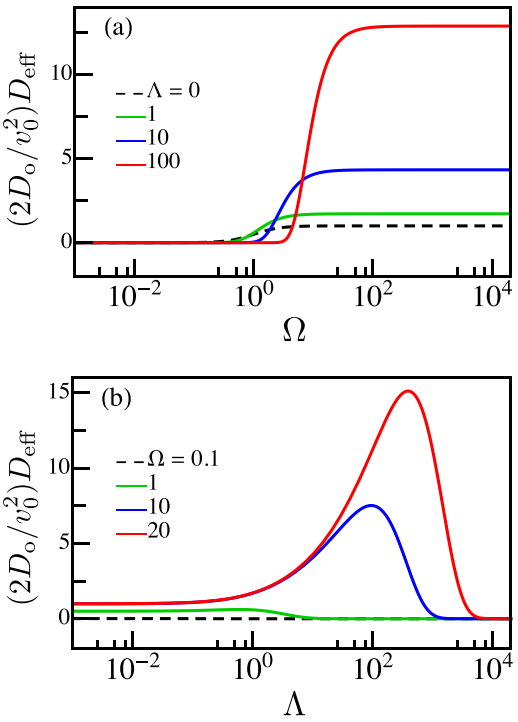

FIG. 4. Dependence of effective diffusivity on rotational Ω and inertia Λ parameters.

$\Omega \gg 1 (D_o \gg |\omega|)$ the self-propeller changes its orientation fast with small steps such that rotational dynamics becomes irrelevant, and in the case of $\Omega \ll 1 (D_o \ll |\omega|)$ the trajectory is close to circular. In both cases the self-propeller follows small steps of displacement and thus small effective diffusivity. In the other limit $\Lambda \gg 1$ the particle's stochastic orientation persists over long times and the trajectories are nearly circular, leading to small effective diffusivities. Between these two limits we have a maximum effective diffusivity whose value increases with increase in Λ. Because in the intermediary regime the trajectories are close to neither circular nor random walk and the length of steps between each orientation change becomes large. Moreover, as shown in Fig. 4(b), the maximum value of $D_{\rm eff}$ occurs at $\Lambda = \Omega^2$ and on increasing Ω, the maximum value increases, and its location shifts to larger Λ. It is clear from Eq. (27b) that in the regime $\lambda \ll 1$ with increase in Λ, the effective diffusivity increases. The other limit $\lambda \gg 1$ has a maximum at $\Lambda = \Omega^2$ (at which $\partial D_{\rm eff}/\partial \Lambda = 0$) and the value of maximum is linearly proportional to Ω. As we discussed in Sec. III in the regime $\Lambda < \Omega^2$ we have two crossovers from ballistic to diffusive to ballistic in the angular dynamics and with increase in Λ, the effective diffusivity increases. In the other regime $\Lambda > \Omega^2$ we only have ballistic behavior in the angular dynamics and effective diffusivity decreases. In other words, $D_{\rm eff}$ originates from coupling between the stochastic noise and deterministic rotation and $\Lambda = \Omega^2$ is the point at which the coupling has the highest effect on $D_{\rm eff}$.

Figure 5 shows the temporal behavior of Eq. (24) for various Λ and Ω values. In all scenarios the dynamics exhibits crossover from a ballistic motion at short times to pure diffusive motion at long times. At short times, where $D_o t \ll \min(1, \Lambda, \Omega)$, i.e., time is shorter than all the timescales, the circular ballistic motion governs the dynamics and MSD $\approx v^2 t^2$ is independent of all timescales. In the limit of $\Omega \ll 1$ $(D_o \ll |\omega|)$, as shown in Fig. 5(a), the deterministic rotational dynamics dominates the orientational diffusivity, and the MSD shows a damped oscillatory behavior. The amplitude of the oscillations increases with increase in orientational memory Λ. We observe spiral patterns in the expected displacement. On the other extreme, $\Omega \gg 1$ $(D_o \gg |\omega|)$, as shown in Fig. 5(b), the orientational diffusion dominates the rotational motion, the propeller changes its direction of motion by stochastic noises fast, and thus the behavior of MSD is qualitatively similar to that of a recltilinear self-propeller with OU processes. In the intermediate regime, $\Omega \approx 1$ $(D_o \approx |\omega|)$, all three timescales can have considerable contributions on the dynamics and we can have damped oscillatory dynamics or nonoscillatory transition from ballistic to diffusive regime, as shown in Fig. 5(c).

VII. CONCLUSION

The orientational memory or, equivalently the rotational inertia, affects both the angular and translational dynamics of an ensemble of rotary self-propellers. In the white-noise limit, the angular dynamics undergo a transition from diffusive to ballistic motion. However, under OU memory, the angular dynamics is either fully ballistic or undergoes two transitions from ballistic to diffusive to ballistic. We showed that the expected displacement of a rotary self-propeller is a spiral in both the white-noise limit and colored-noise scenario. For self-propellers with higher orientational memory this spiral converges at lower rate. Furthermore, deterministic rotation combined with orientational diffusion induces an effective translational diffusion which depends on the noise intensity, the orientational correlation time, and the deterministic

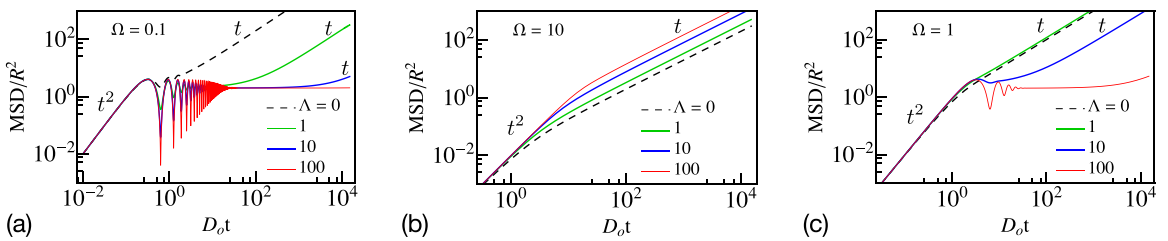

FIG. 5. (a) Damped oscillatory dynamics of MSD in the regime $\Omega \ll 1$ $(D_o \ll |\omega|)$. (b) Nonoscillatory dynamics of MSD in the regime $\Omega \gg 1$ $(D_o \gg |\omega|)$. (c) Intermediate regime with possibilities of damped oscillatory and nonoscillatory dynamics.

rotational dynamics. The effective diffusivity vanishes at both small and large noise intensities, owing to the fact that at these limits, either deterministic rotation or orientational diffusion dominates the other one. We observe a maximum for the effective diffusivity in between the limits.

ACKNOWLEDGMENT

This work was supported by funding from the University of Akron. We are grateful to Paul Lammert for his insightful comments and suggestions.

[1] E. Lauga and T. R. Powers, The hydrodynamics of swimming microorganisms, Rep. Prog. Phys. **72**, 096601 (2009).
[2] M. C. Marchetti, J. F. Joanny, S. Ramaswamy, T. B. Liverpool, J. Prost, M. Rao, and R. A. Simha, Hydrodynamics of soft active matter, Rev. Mod. Phys. **85**, 1143 (2013).
[3] H. C. Berg and R. A. Anderson, Bacteria swim by rotating their flagellar filaments, Nature (London) **245**, 380 (1973).
[4] E. Lauga, Bacterial hydrodynamics, Annu. Rev. Fluid Mech **48**, 105 (2016).
[5] B. M. Friedrich and F. Jülicher, The stochastic dance of circling sperm cells: Sperm chemotaxis in the plane, New J. Phys. **10**, 123025 (2008).
[6] M. Polin, I. Tuval, K. Drescher, J. P. Gollub, and R. E. Goldstein, Chlamydomonas swims with two "gears" in a eukaryotic version of run-and-tumble locomotion, Science **325**, 487 (2009).
[7] D. Selmeczi, L. Li, L. I. Pedersen, S. F. Nrrelykke, P. H. Hagedorn, S. Mosler, N. B. Larsen, E. C. Cox, and H. Flyvbjerg, Cell motility as random motion: A review, Eur. Phys. J. Spec. Top. **157**, 1 (2008).
[8] S. A. Nabavizadeh, J. Castañeda, J. G. Gibbs, and A. Nourhani, Gravitropically stabilized self-assembly of active microcrystallites and spinning free janus particles, Part. Part. Syst. Charact. **39**, 2100232 (2022).
[9] U. K. Cheang, D. Roy, J. H. Lee, and M. J. Kim, Fabrication and magnetic control of bacteria-inspired robotic microswimmers, Appl. Phys. Lett. **97**, 213704 (2010).
[10] J. G. Gibbs, S. Kothari, D. Saintillan, and Y. P. Zhao, Geometrically designing the kinematic behavior of catalytic nanomotors, Nano Lett. **11**, 2543 (2011).
[11] Y. Wang, S. Fei, Y. Byun, P. E. Lammert, V. H. Crespi, A. Sen, and T. E. Mallouk, Dynamic interactions between fast microscale rotors, J. Am. Chem. Soc. **131**, 9926 (2009).
[12] J. R. Howse, R. A. L. Jones, A. J. Ryan, T. Gough, R. Vafabakhsh, and R. Golestanian, Self-Motile Colloidal Particles: From Directed Propulsion to Random Walk, Phys. Rev. Lett. **99**, 048102 (2007).
[13] N. Komin, U. Erdmann, and L. Schimansky-Geier, Random walk theory applied to daphnia motion, Fluct. Noise Lett. **4**, L151 (2004).
[14] S. Bazazi, P. Romanczuk, S. Thomas, L. Schimansky-Geier, J. J. Hale, G. A. Miller, G. A. Sword, S. J. Simpson, and I. D. Couzin, Nutritional state and collective motion: From individuals to mass migration, Proc. R. Soc. B **278**, 356 (2011).
[15] J. Willis, Modelling swimming aquatic animals in hydrodynamic models, Ecol. Modell. **222**, 3869 (2011).
[16] H. S. Niwa, Self-organizing dynamic model of fish schooling, J. Theor. Biol. **171**, 123 (1994).
[17] A. Ordemann, G. Balazsi, and F. Moss, Pattern formation and stochastic motion of the zooplankton daphnia in a light field, Physica A **325**, 260 (2003).
[18] E. Casellas, J. Gautrais, R. Fournier, S. Blanco, M. Combe, V. Fourcassie, G. Theraulaz, and C. Jost, From individual to collective displacements in heterogeneous environments, J. Theor. Biol. **250**, 424 (2008).
[19] G. Theraulaz, J. Gautrais, S. Camazine, and J.-L. Deneubourg, The formation of spatial patterns in social insects: From simple behaviours to complex structures, Philos. Trans. R. Soc. A **361**, 1263 (2003).
[20] M. C. Gonzalez, C. A. Hidalgo, and A.-L. Barabasi, Understanding individual human mobility patterns, Nature (London) **453**, 779 (2008).
[21] D. Helbing, Traffic and related self-driven many-particle systems, Rev. Mod. Phys. **73**, 1067 (2001).
[22] S. van Teeffelen and H. Löwen, Dynamics of a brownian circle swimmer, Phys. Rev. E **78**, 020101(R) (2008).
[23] A. Nourhani, S. J. Ebbens, J. G. Gibbs, and P. E. Lammert, Spiral diffusion of rotating self-propellers with stochastic perturbation, Phys. Rev. E **94**, 030601(R) (2016).
[24] J. G. Gibbs, A. Nourhani, J. N. Johnson, and P. E. Lammert, Spiral diffusion of self-assembled dimers of janus spheres, MRS Adv. **2**, 3471 (2017).
[25] J. Saragosti, P. Silberzan, and A. Buguin, Modeling e. coli tumbles by rotational diffusion. implications for chemotaxis, PLoS ONE **7**, e35412 (2012).
[26] H. C. Berg, Motile behaviour of bacteria, Phys. Today **53**, 24 (2000).
[27] A. Basu, J. F. Joanny, F. Jülicher, and J. Prost, Thermal and non-thermal fluctuations in active polar gels, Eur. Phys. J. E **27**, 149 (2008).
[28] A. Cēbers, Diffusion of magnetotactic bacterium in rotating magnetic field, J. Magn. Magn. Mater. **323**, 279 (2011).
[29] T. Mirkovic, N. S. Zacharia, G. D. Scholes, and G. A. Ozin, Fuel for thought: Chemically powered nanomotors out-swim nature's flagellated bacteria, ACS Nano **4**, 1782 (2010).
[30] R. Dreyfus, J. Baudry, M. L. Roper, M. Fermigier, H. A. Stone, and J. Bibette, Microscopic artificial swimmers, Nature (London) **437**, 862 (2005).
[31] D. A. Fletcher and P. L. Geissler, Active biological materials, Annu. Rev. Phys. Chem. **60**, 469 (2009).
[32] E. Lauga, Life around the scallop theorem, Soft Matter **7**, 3060 (2011).
[33] R. Golestanian, Anomalous Diffusion of Symmetric and Asymmetric Active Colloids, Phys. Rev. Lett. **102**, 188305 (2009).
[34] J. N. Johnson, A. Nourhani, R. Peralta, C. McDonald, B. Thiesing, C. J. Mann, P. E. Lammert, and J. G. Gibbs, Dynamic stabilization of Janus sphere trans-dimers, Phys. Rev. E **95**, 042609 (2017).
[35] F. Thiel, L. Schimansky-Geier, and I. M. Sokolov, Anomalous diffusion in run-and-tumble motion, Phys. Rev. E **86**, 021117 (2012).

[36] P. K. Ghosh, Y. Li, G. Marchegiani, and F. Marchesoni, Communication: Memory effects and active brownian diffusion, J. Chem. Phys. **143**, 211101 (2015).
[37] V. Narayan, S. Ramaswamy, and N. Menon, Long-lived giant number fluctuations in a swarming granular nematic, Science **317**, 105 (2007).
[38] J. D'alessandro, A. Barbier, V. Cellerin, O. Benichou, R. M. Mège, R. Voituriez, B. Ladoux *et al.*, Cell migration guided by long-lived spatial memory, Nat. Commun. **12**, 4118 (2021).
[39] P. Hänggi and P. Jung, Colored noise in dynamical systems, Adv. Chem. Phys. **89**, 239 (2007).
[40] A. Kamenev, B. Meerson, and B. Shklovskii, How Colored Environmental Noise Affects Population Extinction, Phys. Rev. Lett. **101**, 268103 (2008).
[41] H. Löwen, Inertial effects of self-propelled particles: From active brownian to active langevin motion, J. Chem. Phys. **152**, 040901 (2020).
[42] N. Narinder, C. Bechinger, and J. R. Gomez-Solano, Memory-Induced Transition from a Persistent Random Walk to Circular Motion for Achiral Microswimmers, Phys. Rev. Lett. **121**, 078003 (2018).
[43] L. L. Gutierrez-Martinez and M. Sandoval, Inertial effects on trapped active matter, J. Chem. Phys. **153**, 044906 (2020).
[44] J. Su, H. Jiang, and Z. Hou, Inertia-induced nucleation-like motility-induced phase separation, New J. Phys. **23**, 013005 (2021).
[45] J. J. Li and W. Tan, A single dna molecule nanomotor, Nano Lett. **2**, 315 (2002).
[46] A. Najafi and R. Golestanian, Simple swimmer at low reynolds number: Three linked spheres, Phys. Rev. E **69**, 062901 (2004).
[47] W. F. Paxton, J. M. Spruell, and J. F. Stoddart, Heterogeneous catalysis of a copper-coated atomic force microscopy tip for direct-write click chemistry, J. Am. Chem. Soc. **131**, 6692 (2009).
[48] M. Downton, M. Zuckermann, E. Craig, M. Plischke, and H. Linke, Single-polymer brownian motor: A simulation study, Phys. Rev. E **73**, 011909 (2006).
[49] U. Córdova-Figueroa and J. Brady, Osmotic Propulsion: The Osmotic Motor, Phys. Rev. Lett. **100**, 158303 (2008).
[50] T. Fischer and P. Dhar, Comment on "Osmotic Propulsion: The Osmotic Motor," Phys. Rev. Lett. **102**, 159801 (2009).
[51] M. Nabil, S. A. Nabavizadeh, P. E. Lammert, and A. Nourhani, A spectral method for axisymmetric Stokes flow past a particle, J. Fluid. Mech. **936**, R1 (2022).
[52] I. Buttinoni, G. Volpe, F. Kümmel, G. Volpe, and C. Bechinger, Active brownian motion tunable by light, J. Phys.: Condens. Matter **24**, 284129 (2012).
[53] P. Bayati and A. Najafi, Dynamics of two interacting active janus particles, J. Chem. Phys. **144**, 134901 (2016).
[54] R. Ledesma-Aguilar, H. Löwen, and J. M. Yeomans, A circle swimmer at low reynolds number, Eur. Phys. J. E **35**, 70 (2012).
[55] S. van Teeffelen, U. Zimmermann, and H. Löwen, Clockwise-directional circle swimmer moves counter-clockwise in petri dish- and ring-like confinements, Soft Matter **5**, 4510 (2009).
[56] A. Nourhani, P. E. Lammert, A. Borhan, and V. H. Crespi, Chiral diffusion of rotary nanomotors, Phys. Rev. E **87**, 050301(R) (2013).
[57] A. Nourhani, Y. M. Byun, P. E. Lammert, and A. B. V. H. Crespi, Nanomotor mechanisms and motive force distributions from nanorotor trajectories, Phys. Rev. E **88**, 062317 (2013).
[58] F. Kümmel, B. ten Hagen, R. Wittkowski, I. Buttinoni, R. Eichhorn, G. Volpe, H. Löwen, and C. Bechinger, Circular Motion of Asymmetric Self-Propelling Particles, Phys. Rev. Lett. **110**, 198302 (2013).
[59] Y. Sumino, K. H. Nagai, Y. Shitaka, D. Tanaka, K. Yoshikawa, H. Chaté, and K. Oiwa, Large-scale vortex lattice emerging from collectively moving microtubules, Nature (London) **483**, 448 (2012).
[60] L. Caprini and U. M. B. Marconi, Active chiral particles under confinement: Surface currents and bulk accumulation phenomena, Soft Matter **15**, 2627 (2019).
[61] F. J. Sevilla, Diffusion of active chiral particles, Phys. Rev. E **94**, 062120 (2016).
[62] K. S. Olsen, Diffusion of active particles with angular velocity reversal, Phys. Rev. E **103**, 052608 (2021).
[63] A. R. Sprenger, S. Jahanshahi, A. V. Ivlev, and H. Löwen, Time-dependent inertia of self-propelled particles: The langevin rocket, Phys. Rev. E **103**, 042601 (2021).
[64] W. R. DiLuzio, L. Turner, M. Mayer, P. Garstecki, D. B. Weibel, H. C. Berg, and G. M. Whitesides, Escherichia coli swim on the right-hand side, Nature (London) **435**, 1271 (2005).
[65] I. H. Riedel, K. Kruse, and J. Howard, Science **309**, 300 (2005).
[66] E. Lauga, W. R. Diluzio, G. M. Whitesides, and H. A. Stone, Swimming in circles: Motion of bacteria near solid boundaries, Biophys. J. **90**, 400 (2006).
[67] L. Lemelle, J.-F. Palierne, E. Chatre, and C. Place, Counter-clockwise circular motion of bacteria swimming at the air-liquid interface, J. Bacteriol. **192**, 6307 (2010).
[68] P. Bayati, M. N. Popescu, W. E. Uspal, S. Dietrich, and A. Najafi, Dynamics near planar walls for various model self-phoretic particles, Soft Matter **15**, 5644 (2019).
[69] P. Bayati and A. Najafi, Electrophoresis of active janus particles, J. Chem. Phys. **150**, 234902 (2019).
[70] J. G. Gibbs and Y. P. Zhao, Design and characterization of rotational multicomponent catalytic nanomotors, Small **5**, 2304 (2009).
[71] S. Ye and R. L. Carroll, Design and fabrication of bimetallic colloidal "janus" particles, ACS Appl. Mater. Interfaces **2**, 616 (2010).
[72] N. A. Marine, P. M. Wheat, J. Ault, and J. D. Posner, Diffusive behaviors of circle-swimming motors, Phys. Rev. E **87**, 052305 (2013).
[73] C. Weber, P. K. Radtke, L. Schimansky-Geier, and P. Hänggi, Active motion assisted by correlated stochastic torques, Phys. Rev. E **84**, 011132 (2011).
[74] A. Nourhani, V. H. Crespi, and P. E. Lammert, Gaussian memory in kinematic matrix theory for self-propellers, Phys. Rev. E **90**, 062304 (2014).
[75] A. Nourhani, P. E. Lammert, A. Borhan, and V. H. Crespi, Kinematic matrix theory and universalities in self-propellers and active swimmers, Phys. Rev. E **89**, 062304 (2014).